analytical chemistry

Article

MALDI-2 for the Enhanced Analysis of *N*-Linked Glycans by Mass Spectrometry Imaging

Bram Heijs,* Alexander Potthoff, Jens Soltwisch, and Klaus Dreisewerd

Cite This: *Anal. Chem.* 2020, 92, 13904−13911

Read Online

ACCESS | Metrics & More | Article Recommendations | SI Supporting Information

ABSTRACT: *N*-glycans are important players in a variety of pathologies including different types of cancer, (auto)immune diseases, and also viral infections. Matrix-assisted laser desorption/ionization mass spectrometry (MALDI-MS) is an important tool for high-throughput *N*-glycan profiling and, upon use of tandem MS, for structure determination. By use of MALDI-MS imaging (MSI) in combination with PNGase F treatment, also spatially correlated *N*-glycan profiling from tissue sections becomes possible. Here we coupled laser-induced postionization, or MALDI-2, to a trapped ion mobility quadrupole time-of-flight mass spectrometer (timsTOF fleX MALDI-2, Bruker Daltonics). We demonstrate that with MALDI-2 the sensitivity for the detection of molecular $[M − H]^−$ species of *N*-glycans increased by about 3 orders of magnitude. Compared to the current gold standard, the positive ion mode analysis of $[M + Na]^+$ adducts, a sensitivity increase by about a factor of 10 is achieved. By exploiting the advantageous fragmentation behavior of $[M − H]^−$ ions, exceedingly rich structural information on the composition of complex *N*-glycans was moreover obtained directly from thin tissue sections of human cerebellum and upon use of low-energy collision-induced dissociation tandem MS. In another set of experiments, in this case by use of a modified Synapt G2-S QTOF mass spectrometer (Waters), we investigated the influence of relevant input parameters, in particular pressure of the N_2 cooling gas in the ion source, delay between the two laser pulses, and that of their pulse energies. In this way, analytical conditions were identified at which molecular ion abundances were maximized and fragmentation reactions minimized. The use of negative ion mode MALDI-2-MSI could constitute a valuable tool in glycobiology research.
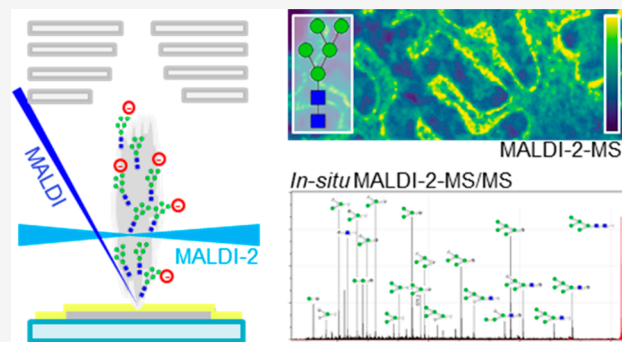
Matrix-assisted laser desorption/ionization mass spectrometry (MALDI-MS) is a popular tool for high-throughput analysis of oligosaccharides including N- and O-linked glycans. Typically, the oligosaccharides are derived from glycoproteins by enzymatic, or in the case of O-linked glycans, chemical cleavage (e.g., PNGase F or β-elimination). MALDI-MS has been used to profile glycans from a variety of biological matrices, including biofluids such as serum, blood, and urine, as well as other matrices (e.g., food sources and plant material).[1−6] To also reveal important spatial information on glycans in tissue, MALDI-MS imaging (MALDI-MSI) can be used.[7,8] Application examples of MALDI-MSI comprise, for example, the role specific glycosylation patterns play in the development and pathogenesis of ovarian and breast cancer and myxoid liposarcoma.[9−13]

Because of the better detection sensitivity, the majority of these applications relied on the detection of singly charged alkali-metal adduct ions, typically $[M + Na]^+$. For structure elucidation, low-energy collision-induced dissociation (CID) is commonly used and in positive ion mode typically results in fragmentation of the glycosidic bond, with little formation of cross-ring fragments. In contrast, CID in negative ion mode predominantly yields diagnostic cross-ring fragments required

for the unambiguous identification of intersaccharide linkages. Therefore, negative ion mode MS finds its application mostly in tandem MS analysis of oligosaccharides.[14−16] A hindrance for more extensively exploiting this potential is given by the rather low ion yields of MALDI for oligosaccharides in the negative ion mode. Therefore, a plethora of derivatization strategies has been developed to stabilize and neutralize the notoriously labile terminal sialic acid residues,[17−19] as well as functionalize the reducing end of the oligosaccharide with a stabilizing, often fluorescent, and permanently charged group.[19−21] Although functional, these strategies often result in complex sample preparation protocols, which are prone to the inclusion of experimentally induced measurement variations. Moreover, chemical derivatization strategies are not always transferable to
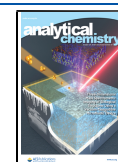
tissue sections, and therefore they may not be applicable to MALDI-MSI.

A powerful alternative to increase the ion yields of deprotonated oligosaccharides is MALDI-MS coupled with laser-induced postionization (PI), or MALDI-2-MSI.[22] With this recently introduced technique, the initial MALDI-particle plume, which is formed in a fine vacuum environment of a few mbar of N_2, is intercepted by the beam of a pulsed PI-laser (e.g., a q-switched Nd:YAG laser emitting at 266 nm[23]) a suitable distance and interlaser pulse delay. Very recently, also the first successful adaptation of MALDI-2 in combination with an atmospheric pressure (AP) ion source has been reported.[24] Somewhat depending on matrix, analyte, spot size, and pulse energy of the ablation laser, optimal MALDI-2 conditions are typically found if a central distance of the PI laser beam to the primary laser spot of about 500 μm and an interlaser pulse delay of ~10 μs are established (see the Results and Discussion section below). The interaction of the PI laser beam with the particle plume gives rise to a significant boost in ion yields for numerous classes of small molecules but also for more complex lipids like phospho- and glycosphingolipids. The current hypothesis on the working mechanism of MALDI-2, based predominantly on studies that were performed with glycerophospholipids, consists of two coexisting mechanisms.[25] The first is based on resonance-enhanced two-photon ionization (REMPI) of the MALDI matrix. For aromatic MALDI matrices, this condition is generally met for wavelengths shorter than 310 nm. Because of energetically favorable reactions, the newly formed charges are transferred to neutral analytes in close proximity, presumably via gas phase collisions. Additionally, a mechanism similar to aerosol MALDI[26] could result in a more conventional MALDI process upon involvement of larger clusters. Further work is needed to elucidate these pathways for different combinations of MALDI matrices and laser parameters.[22,25,27,28]

The application of MALDI-2 to the analysis of oligosaccharides in negative ion mode could potentially simplify sample preparation workflows and enhance ion yields and would therefore improve reproducibility and sensitivity of the analysis. While already indicated by an increase in signal intensity for small disaccharides (Hex2) by Soltwisch et al., beneficial effects for the analysis of larger, more complex oligosaccharides can, however, currently only be suspected.[22] Therefore, we have studied these potential benefits of applying MALDI-2 for mass spectrometry-based glycomics approaches and N-glycan MSI at the examples of a set of standards and by the analysis of human brain sections at 50 μm pixel sizes. We also tested the potential of low-energy CID tandem MS for generating structurally informative fragments from $[M - H]^-$ precursors of complex N-glycans directly from human brain tissue.

■ MATERIALS AND METHODS

Chemicals and Reagents. Acetonitrile (ACN) and LC-MS-grade deionized water (dH$_2$O) were acquired from Carl ROTH (Karlsruhe, Germany). *Nor*-harmane (NOR), histological grade xylene, and Millipore Amicon Ultra-0.5 centrifugal filter units (10 kDa molecular-weight cutoff (MWCO) filters) were obtained from Sigma-Aldrich (Steinheim, Germany). Ethanol (EtOH) and 2,5-dihydroxyacetophenone (2,5-DHAP) were acquired from Merck (Darmstadt, Germany). Oligosaccharide standards (Maltoheptaose DP7 (DP7); N-glycan H5N4) were obtained from Biosynth Carbosynth (Compton, U.K.). Endoglycosidase PNGase F, recombinant (lyophilized) (Serva Electrophoresis, Heidelberg, Germany),

and ESI-L low concentration tuning mix (Agilent Technologies, Santa Clara, CA, U.S.A.) were acquired at the indicated vendors. Superfrost microscope glass slides were acquired from Thermo Scientific (Schwerte, Germany).

Tissues and Tissue Treatment. Formalin-fixed and paraffin-embedded (FFPE) human brain (cerebellum region) tissue obtained from a 79-year-old male were obtained from the Department of Neuropathology of the University Hospital Münster (UKM). The individual died from cardiovascular disease without known neurological disorders. Tissues were sectioned at 5 μm thickness and were mounted on Superfrost glass slides (Thermo Scientific). Sections were stored at 4 °C in the dark until further processing. Tissues were used following in accordance with the research ethics board approval (1IIIPau; UKM, Münster, Germany).

Maltoheptaose Sensitivity Measurements. Sensitivity measurements for the MALDI-2-MS analysis of oligosaccharides were assessed using a timsTOF fleX MALDI-2 QTOF instrument (Bruker Daltonics; details on the performed modifications are provided in the Supporting Information) and in ref 29. Spectra (n = 5), recorded over an m/z-range of 500−1500, were acquired in positive ion mode using MALDI, and in negative ion mode both with and without MALDI-2; MALDI-2 in the positive ion mode was also tried but did not result in sizable differences in the ion abundances of the $[M + Na]^+$ ions, and was therefore not used anymore in further experiments. Spectra (400 laser shots summed) were acquired at optimized settings: 3.0 mbar cooling gas pressure (N_2), 50 × 50 μm^2 pixel size ("M5 small" setting, ablation surface 1280 μm^2), approximately 22 μJ or 52 μJ ablation laser pulse energies in positive and negative ion mode, respectively. All spectra were recorded using 1 kHz repetition rates for both ablation and PI lasers. For the MALDI-2 measurements in negative ion mode, approximately 350 μJ PI-laser pulse energy, and an interlaser pulse delay of 30 μs were used.

***N*-Glycan MALDI-2-MSI Sample Preparation and Analysis.** FFPE sections were dewaxed using two 10 min-long washes in xylene. Following dewaxing, tissues were rehydrated in a series of EtOH washes (100% EtOH (3×), 70% EtOH (1×), 50% EtOH (1×), dH$_2$O (1×), 1× equals 20 2 s dips) and washed in dH$_2$O for an additional 5 min. Samples were dried under a stream of N_2. Endoglycosidase PNGase F was buffer exchanged using 10 kDa MWCO filters, dissolved in dH$_2$O (0.1 μg μL^{-1}), and homogeneously applied on the tissue sections using the SimCoat spray-robot (SonoTek; 40 passes; flow rate, 30 μL min^{-1}; XY-stage-speed, 30 mm s^{-1}; line-to-line distance, 1.8 mm; ultrasound power (at 48 kHz), 1.5 W). Tissues were incubated overnight (18 h) at 37 °C in a saturated humid environment. Following incubation 41 mM NOR, and 5 μM maltoheptaose (in 50:50 (% v/v) ACN:dH$_2$O) were cosprayed on the tissue using the following parameters: 40 passes; flow rate, 50 μL min^{-1}; XY-stage-speed, 30 mm s^{-1}; line-to-line distance, 1.8 mm; ultrasound power, 6.0 W (at 48 kHz). Unless otherwise noted, MALDI-2-MSI was performed on the timsTOF fleX MALDI-2 (Bruker Daltonics) in negative ion mode at optimized conditions: N_2 cooling gas pressure, 3.0 mbar; ablation laser pulse energy, 34 μJ; interlaser pulse delay, 30 μs; PI laser pulse energy, 350 μJ; 50 laser shots per pixel. For the analyses assessing the influence of cooling gas pressure and interlaser pulse delay, the respective parameters were adjusted accordingly, while all other parameters were kept identical. Positive ion mode MALDI-MSI measurements were performed after applying 46 mM 2,5-DHAP and 5 μM maltoheptaose (in

50:50 (% v/v) ACN:dH$_2$O) using the same spraying method used for applying NOR. Spectra were recorded at p = 3.0 mbar, using an ablation laser pulse energy of 34 μJ, and 500 shots per pixel. All spectra were recorded using 1 kHz repetition rates for both ablation and PI lasers, and over an m/z range between 900 and 3000 using a 50 $\times$ 50 μm^2 pixel size ("M5 small"). After acquisition, data was imported and analyzed in SCiLS Lab MVS (2020a Pro, build 8.00.11593, Bruker Daltonics). Figures were prepared in Prism (8.1.1, build 330, GraphPad), mMass (5.5.0, www.mmass.org), and the Office 2016 software suite (Microsoft).

RESULTS AND DISCUSSION

MALDI-2 of Oligosaccharides in Positive and Negative Ion Modes. First, we assessed whether the MALDI-MS-based detection of oligosaccharides can be improved by applying MALDI-2 with the analyses of oligosaccharide standards and then with endogenous N-glycans from tissue sections. Our goal was to study key effects of the MALDI-2 parameters, and not least to optimize experimental protocols for MALDI-2-MS(I) of N-glycans.

The intensities of the ablation and PI laser were systematically varied to study their effects on the (post)ionization of the oligosaccharide. In positive ion mode, the sodium adducts of maltoheptaose did not benefit from MALDI-2, and even decreased somewhat (by up to a factor of 3) with increasing PI-laser energy (Figure 1A). This observation is in line with previously published observations on lipids, where decreased MALDI-2 signal intensities of sodium adducts have been hypothesized to be an effect of either the elevated pressure in the ion source, leading to suboptimal ion transmission conditions, or increased de novo formation of negative ion species during the MALDI-2 procedure, having a neutralizing effect on positive ion species.[25,30] The results displayed here led us to believe that these observations are not analyte class specific. Similar to the reports on MALDI-2 of lipids, the protonated maltoheptaose ion received a boost in signal intensity. However, to achieve this effect high ablation laser energies were required, which resulted in partial dissociation of maltoheptaose via the loss of single or more hexose units (Figure S1A,B, Supporting Information). The option to boost protonated molecular ions of oligosaccharides should perhaps be studied further in the future (e.g., by using different matrix systems).

In the negative ion mode, a clear boost in signal intensity as a function of increasing PI-laser energy was observed for the deprotonated maltoheptaose molecule. However, it is well-known that [M−H]$^-$ ions of neutral oligosaccharides are prone to in-source dissociation (ISD) - these fragment peaks were indeed detected in both MALDI and MALDI-2 analyses (Figure S1C,D, Supporting Information). However, under identical conditions (besides applying PI) the intensity of the intact maltoheptaose ion was enhanced much stronger by MALDI-2 compared to its ISD fragments (Figure S2, Supporting Information). Previously, several groups successfully stabilized deprotonated oligosaccharide ions by adding sodium iodide to the MALDI matrix and therefore promote the formation of iodide adducts.[31,32] This strategy did not result in increased MALDI-2 signals in negative (data not shown), which is in line with the findings on detection of adducts in positive ion mode described earlier.

Optimization of MALDI-2 Parameters. To address this and further mechanistic questions, next we studied the effects of the experimental parameters of MALDI-2 with a focus on the
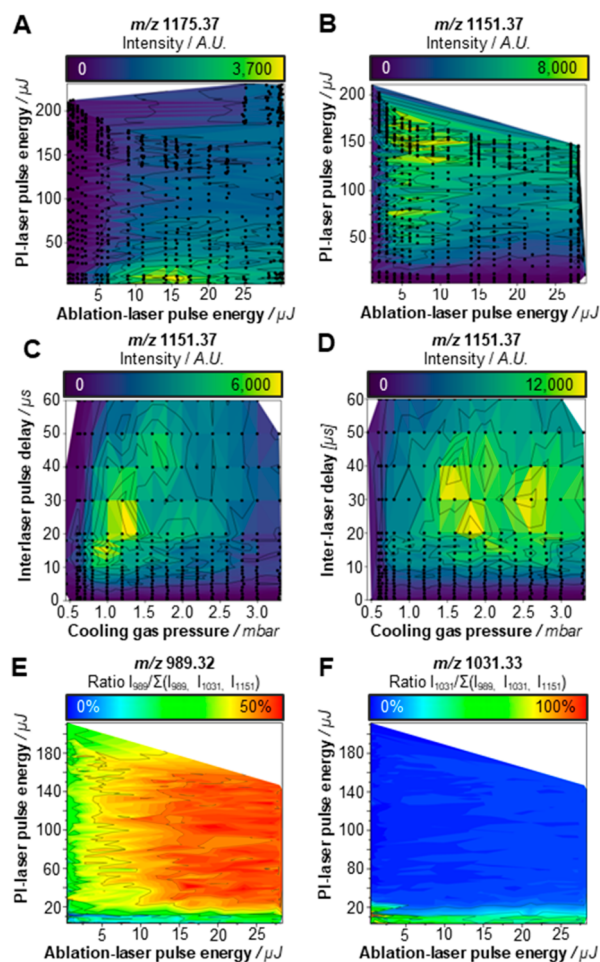
Figure 1. Optimization of PI parameters in negative ion mode MALDI-2 measurements. The influence of the ablation and PI-laser pulse energies (at a fixed cooling gas pressure of 2.0 mbar, and an interlaser pulse delay of 10 μs) on the signal intensity of (A) the [M + Na]$^+$ signal of maltoheptaose (m/z 1175.37) and (B) the [M − H]$^-$ signal of the oligosaccharide (m/z 1151.37 [maltoheptaose − H]$^-$). Additionally, the effects of cooling gas pressure, and the interlaser pulse delay on the signal intensity of deprotonated maltoheptaose molecules were assessed. Spectra were acquired using an ablation-laser pulse energy of (C) 5 and (D) 25 μJ, respectively. PI-laser pulse energy was at the maximum energy of approximately 200 μJ. Common for the MALDI-based analysis of neutral oligosaccharides, in-source fragmentation occurred. Different types of fragments were produced under different conditions; in panels A−D, black dots represent individual measurements (average of n = 10 pixels). (E) Loss of a hexose (m/z 989.32 [maltoheptaose−C$_6$H$_{10}$O$_5$−H]$^-$) occurred predominantly under MALDI-2 conditions (using both high ablation laser, and PI energies). (F) Higher-energy cross-ring saccharide fragmentation (m/z 1031.33 [maltoheptaose−C$_4$H$_8$O$_4$− H]$^-$) occurred exclusively under normal MALDI-conditions, and even at low ablation laser energies. Relative fragmentation (E and F) was calculated as the fragment-intensity over the sum of intact maltoheptaose and all detected fragments.

negative ion mode analysis. By varying τ and p in combination with a relatively "low" ablation laser pulse energy, not far from the ion detection threshold, we observed two sets of conditions, or regimes, that resulted in increased maltoheptaose ion yields (Figure 1C): regime (i) 0.5 mbar < p < 1 mbar and 10 μs < τ < 20 μs and regime (ii) 1.0 mbar < p < 1.5 mbar and 20 μs < τ < 30 μs.

At high ablation laser pulse energy conditions (Figure 1D), the highest maltoheptaose intensities were found at elevated

pressure (1.5 mbar < p < 3.0 mbar) and 20 μs < τ < 40 μs. The maximum absolute intensity of the deprotonated maltoheptaose ion in the high ablation laser pulse energy experiment was doubled compared to the intensity recorded at low ablation laser pulse energy. At both low and high ablation laser pulse energy settings, fragmentation occurred predominantly at low pressure (p < 1 mbar) and short interlaser pulse delay (10 μs < τ < 20 μs) conditions (Figure S3A,B, Supporting Information). These results indicate the presence of (at least) two ion populations following the MALDI event. One being a population of molecular ions exhibiting a high mean velocity, generated (most likely) through a "thermal" desorption process,[33] and one slower population with larger clusters, ejected from the tissue surface through an ablation mechanism. Very similar findings were obtained through modeling MALDI-plume development by Knochenmuss[34] and have been experimentally described by Niehaus and Soltwisch for glycerophospholipids and glycolipids,[27] as well as by other authors for various analyte/matrix systems and summarized in a review by Dreisewerd.[35]

Next, we asked if the negative ion mode MALDI-2-MSI mechanisms, as revealed with the maltoheptaose standards, may also apply for more complex glycans, namely enzymatically released *N*-glycans. To account for possible tissue-type (and area)-dependent variations in ion suppression effects,[28,36–39] we homogeneously sprayed maltoheptaose (5 μM) onto human cerebellum tissues and recorded MALDI-2-MSI data at a set of different p (between 2.0−3.0 mbar, Figure S4A, Supporting Information) and τ (between 5−60 μs, Figure S4D, Supporting Information) values. The $[M - H]^-$ maltoheptaose signals were used for normalization.

As for the pure maltoheptaose samples, the MALDI-2-MSI data again show a strong pressure dependence on the oligosaccharide/glycan signal intensity. Higher pressures, as well as an optimal interlaser pulse delay around 30 μs were found favorable for the analysis of *N*-glycans from tissue. However, the effect of the interlaser pulse delay on the signal intensity was much less pronounced than for the sample system above.

In-Source Dissociation in the Negative Ion Mode. Next, we recommended to ask if fragmentation of oligosaccharides was increased by the MALDI-2 process or whether it rather results from the MALDI process, and fragment signals were merely enhanced by MALDI-2. We found that the relative majority of cross-ring fragmentation occurred under MALDI conditions (no PI-laser energy applied; Figure 1E). Similar to the observations in the positive ion mode, dissociation of the glycosidic bond resulting in the loss of a complete hexose residue, occurred predominantly as an effect of increased ablation-laser energy (Figure 1F). Also, in the MALDI-2-MSI analyses, we detected fragment ions (cross-ring as well as loss of hexose) for both the homogeneously sprayed maltoheptaose internal standard, and endogenous *N*-glycans. When varying the cooling gas pressure, the absolute intensities of the fragments followed the same trends as the intact endogenous glycan (Figure S4B, SI), but the relative abundances of fragments and intact oligosaccharide remained the same (Figure S4C, SI). Similar observations were made when changing the interlaser pulse delay (Figure S4E,F, SI). However, while the relative abundance of the intact glycan did not change much under the influence of τ, there were relative changes between the type of fragments that were favored between short and longer interlaser pulse delays (Figure S4F, SI). Short interlaser pulse delays resulted predominantly in the formation of cross-ring fragments, while longer interlaser pulse delays favored glycosidic bond

fragmentation. As cross-ring fragmentation generally requires more fragmentation energy, and short interlaser pulse delays result in PI of faster, high-energy single ions formed through "thermal" desorption, these observations fit very well with the presence of multiple ion populations in the MALDI plume described above. Moreover, from these data we were able to finally conclude that the observed in-source fragmentation is mainly generated in the ablation process. The MALDI-derived fragment ions were enhanced by MALDI-2, but under the tested conditions no additional fragmentation induced by the second laser pulse seemed to occur.

Improved MALDI-2 Measurement Sensitivity. Although $[M-H]^-$ signal increases were observed for negative ion mode MALDI-2 measurements, the ultimate question was whether the signal increase would translate to an increase in measurement sensitivity for MALDI-2. Therefore, a maltoheptaose dilution series was prepared and analyzed in positive ion mode without PI, and in negative ion mode both with and without PI. Due to the homogeneous preparation, and the high pixel fidelity of the timsTOF fleX, the amount of maltoheptaose per 50 × 50 μm^2 pixel could be calculated (Supplementary Table S-1, Supporting Information). In negative ion mode, MALDI-2 analysis (Figure 2A) resulted in the smallest lower limit of detection (LLOD) of 2 amol per pixel. This LLOD improved by 3 orders of magnitude
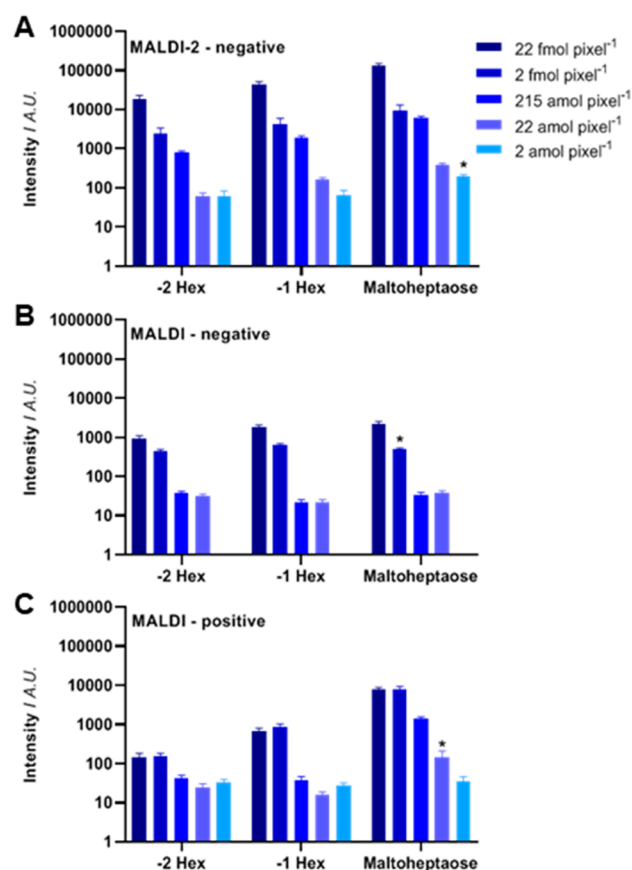
Figure 2. Oligosaccharide sensitivity. A dilution series of spraycoated maltoheptaose on glass slide was analyzed by (A) MALDI-2-MS in negative ion mode, (B) MALDI-MS in negative ion mode, and (C) MALDI-MS in positive ion mode. The bars show the mean intensity of the performed experiments ($n = 5$). Asterisks (*) highlight the lower limit of detection (signal-to-noise ratio (SNR) ≥ 3), and error bars represent the SEM.
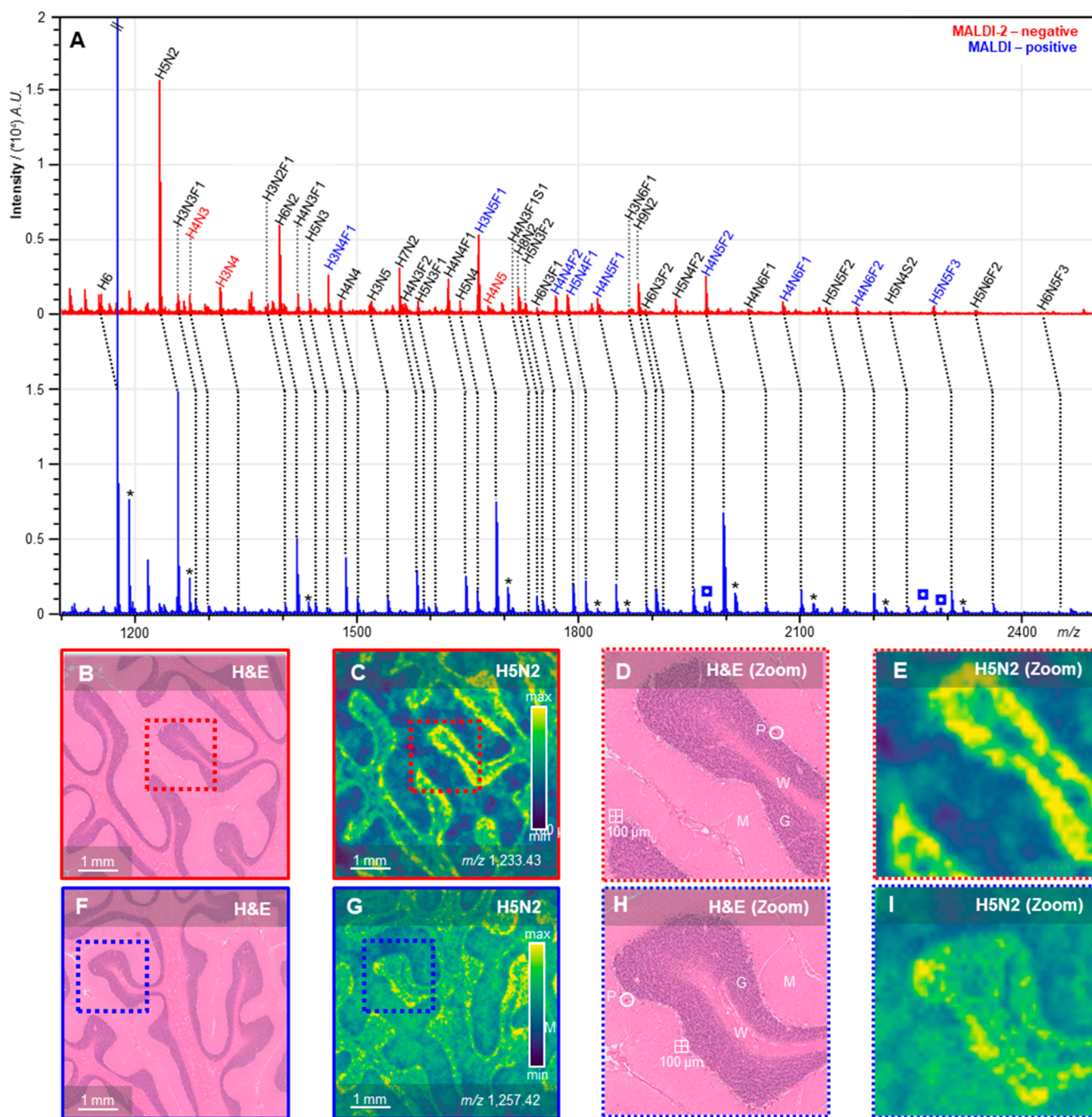
Figure 3. Spectra and images of positive-ion mode MALDI-MSI and negative ion-mode MALDI-2-MSI. (A) Average spectra for negative ion-mode MALDI-2-MSI (red) and positive ion-mode MALDI-MSI (blue) with assigned *N*-glycan species. Colored *N*-glycan compositions represent a > ± 10% variation of intensity between positive and negative ion-mode analyses. Peaks with an asterisk (*) in the positive ion mode spectrum are potassium adducts. (B,F) H&E stained consecutive section displaying cerebellar brain morphology. (C,G) Example images for *N*-glycan H5N2 in human cerebellum. (D,H) Zoom in on histology with different morphological structures annotated (P, Purkinje cell, G, granular layer, M, molecular layer, W, white matter). (E,I) Zoom in on example H5N2 images. In red, negative ion-mode MALDI-2-MSI images, and in blue, positive ion-mode MALDI-MSI images.

in the equivalent negative ion mode measurement without MALDI-2 (LLOD: 2 fmol per pixel; Figure 2B) and 1 order of magnitude in the positive ion mode MALDI measurements of the maltoheptaose sodium adduct (LLOD: 22 amol per pixel; Figure 2C). Further studies are required to assess whether similar performance benefits are achieved for various glycan classes, and for in situ analysis from tissue.

N-Glycan MALDI-2-MSI. To evaluate whether ion species generated from the same *N*-glycans in both positive ion mode

MALDI and negative ion mode MALDI-2 would show the same profiles and spatial distributions in tissue, a comparison experiment was performed on human cerebellum tissues. Figure 3A shows the represetative average tissue spectra obtained from the two analyses. Tissue analysis using negative ion mode MALDI was also attempted, but the resulting spectra were of such poor quality that the MSI data would only comprise of noise. Due to the ISD in the negative ion mode, there seems to be a slight bias toward the smaller *N*-glycans in the MALDI-2-
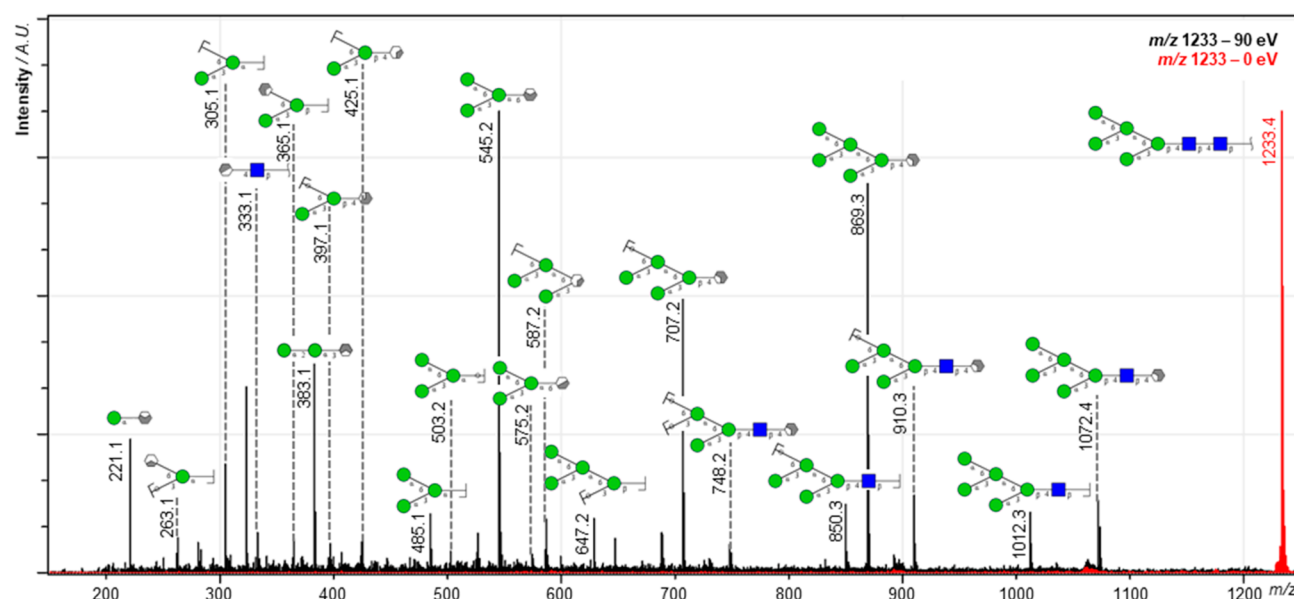
Figure 4. MALDI-2 tandem MS spectrum of deprotonated H5N2 from human cerebellum. The red trace shows a pseudo-MS1 spectrum, where quadrupole filtering was applied but no collision energy (0 eV). The black trace shows the low-energy CID MS/MS spectrum that resulted by applying a collision energy of 100 eV (laboratory frame). Both spectra were acquired from a total of 20 50×50 μm^2 wide pixels from a human cerebellum tissue previously analyzed by MALDI-2-MSI. Based on mass matching (mass error tolerance, ± 10 ppm), the majority of high intensity peaks could be assigned with fragment identities. Note that the applied method, which is not incorporating the use of ion mobility spectrometry, does not allow for separation of isomeric fragments. For visualization, only one hypothetical isomer is therefore denoted. Blue squares represent N-acetylhexoses (HexNAc), green circles represent hexoses (Hex), and grayish hexagons represent various additional cross-ring fragments.

MSI analysis. The affected glycans with an intensity variation more than $> \pm 10\%$ have been highlighted. However, as can be deduced from Figure 3B−I, the recorded distributions showed the same glycans to be present in similar morphological areas upon measurement with the two ion polarities.

One striking observation is that, although varying notably in their structural composition, the majority of the registered N-glycans express very similar expression profiles across the investigated brain area (Figure S5, Supporting Information). Presumably due to the general difficulty to access human brain samples for these analytical purposes, we could not find any previous MALDI-MSI-based data for N-glycans in the human cerebellum in the literature for comparison. However, both the Human Protein Atlas (http://www.proteinatlas.org) and the Allen Mouse Brain Atlas (http://www.brain-map.org) contain data on the expression of key-enzymes of the N-glycan biosynthesis pathway. Mannosidase 1, alpha (*man1a1*) is the enzyme responsible for trimming H9N2 to H8N2 in the endoplasmatic reticulum (ER). As it is one of the "early-stage" enzymes of the biosynthesis pathway, all N-glycans that are expressed have been processed by this enzyme, and therefore it is a good marker for the presence of N-glycosylated proteins. We found *man1a1* to be predominantly expressed in the Purkinje cell layer in both human and mouse cerebellum (Figure S6, Supporting Information). Additional expression was found in the granular layer, although at lower levels compared to the Purkinje cells. These findings correspond well to the distributions found for the N-glycans detected by MSI. Especially the negative ion mode MALDI-2 analysis showed a very clear delineation of the Purkinje cells and granular layer in all of the recorded glycan distributions (Figures 3 and S5, Supporting Information).

An additional benefit of the analysis of oligosaccharides in the negative ion mode is the absence of peak-splitting that occurs in

positive ion mode through the presence of multiple alkali-metal adducts for the same glycan (e.g., sodium and potassium adducts; Figure 3A). In MALDI-MSI experiments, local differences in salt concentrations can affect adduct formation, which will ultimately result in biased (semi)quantitative data.[40,41] Although additional research is needed to assess potential differences in (post)ionization efficiencies of various glycan classes (e.g., high-mannose vs complex-type, sialylated and/or fucosylated species), in our view, these results show clearly that MALDI-2-MSI can be an exceedingly useful tool for the visualization of N-glycans in FFPE tissue sections.

In Situ MALDI-2-MS/MS. In mass spectrometry-based glycomics, the negative ion mode is commonly used for obtaining tandem MS spectra, as they contain unique isomer-specific cross-ring fragment ion signals not readily available in positive ion mode.[31,42,43] In previous MSI-based studies on N-glycans, oligosaccharide compositions were determined based on mass-matching, often in combination with the off-tissue analysis of extracts by MALDI-MS/MS.[17,43] This indirect, and laborious approach is often required as the sensitivity of MALDI-MS/MS is generally too low for structure elucidation directly from tissue.

In our initial study, highlighting the general capabilities of the timsTOF fleX MALDI-2 instrument, we already included examples for the in situ MS/MS analysis of (glyco-)lipids recorded from murine tissue.[29] Here we show that with this instrument similar advancement are achieved for on-tissue MS/MS of N-glycans. In total the identity of 14 out of the 38 tentatively assigned N-glycan species as observed in the MALDI-2-MSI analysis (Figure 3) was confirmed by MALDI-2-MS/MS directly from the previously analyzed tissue section (Table S2, Supporting Information). Figure 4 shows an example of an on-tissue MS/MS spectrum from H5N2, obtained using MALDI-2 in the negative ion mode. Consistent with work by Harvey,

where MS/MS analyses of electrosprayed $[M-NO_3]^-$ and $[M-(NO_3)_2]^{2-}$ ions from neutral high-mannose N-linked glycans and their 2-aminobenzamide derivatives was performed, the most abundant fragment peaks were present in the analyzed spectra.[44]

CONCLUSIONS

MALDI-2 performed in the negative ion mode induces a boost in $[M-H]^-$ ion yields for the analysis of oligosaccharides. As a result, this provides an order of magnitude higher sensitivity compared to the current "gold standard", the positive ion mode MALDI analysis of sodium-adducts of oligosaccharides. In the mechanistic part of our study, we moreover optimized several key parameters for MALDI-2-MSI of N-glycans in the negative ion mode. Using the so optimized conditions, we showed how the increased ion yields could be highly beneficial for the acquisition of high-quality MS/MS spectra and structural analysis of N-glycans from minute sample amounts. Although having a focus on N-glycans and neutral standards (maltoheptaose), we foresee that the method will also reach out beyond these systems. It could, for instance, also comprise valuable for O-glycan analysis. And, although not studied in the context of this manuscript, making use of the trapped ion-mobility separation (TIMS) capabilities of the timsTOF fleX MALDI-2 instrument, valuable information on the presence and distribution of N-glycan isomers in tissue is expected to benefit strongly from MALDI-2. In summary, MALDI-2 could comprise a valuable tool for many applications in mass spectrometry-based glycomics research.

ASSOCIATED CONTENT

Supporting Information

The Supporting Information is available free of charge at https://pubs.acs.org/doi/10.1021/acs.analchem.0c02732.

> Supplementary methods; supplementary references; supplementary figures showing: the effect of laser pulse energies on the fragmentation of oligosaccharides; the effect of MALDI-2 and negative ion mode on oligosaccharide fragmentation; the effect of cooling gas pressure and interlaser pulse delay on fragmentation; the effect of cooling gas pressure and interlaser pulse delay on MSI of N-glycans in human cerebellum tissue; comparison of example images of various N-glycans between negative ion mode MALDI-2-MSI and positive ion mode MALDI-MSI; mannosidase 1, alpha expression in human and mouse brain (PDF)

> Supplementary table with a fragment database from the in situ tandem MS analyses of release endogenous N-glycans (XLSX)

AUTHOR INFORMATION

Corresponding Author

Bram Heijs − Institute of Hygiene, University of Münster, 48149 Münster, Germany; Center for Proteomics and Metabolomics, Leiden University Medical Center, 2333 ZA Leiden, The Netherlands; orcid.org/0000-0001-6328-9305; Email: b.p.a.m.heijs@lumc.nl

Authors

Alexander Potthoff − Institute of Hygiene, University of Münster, 48149 Münster, Germany

Jens Soltwisch − Institute of Hygiene and Interdisciplinary Center for Clinical Research (IZKF), University of Münster, 48149 Münster, Germany; orcid.org/0000-0002-0258-1561

Klaus Dreisewerd − Institute of Hygiene and Interdisciplinary Center for Clinical Research (IZKF), University of Münster, 48149 Münster, Germany; orcid.org/0000-0002-7619-808X

Complete contact information is available at:
https://pubs.acs.org/10.1021/acs.analchem.0c02732

Author Contributions

The manuscript was written through contributions of all authors. All authors have given approval to the final version of the manuscript.

Notes

The authors declare the following competing financial interest(s): B.H. was supported by Bruker Daltonics during the course of this project. All other authors declare no conflict of interest.

REFERENCES

(1) Hall, P. L.; Lam, C.; Alexander, J. J.; Asif, G.; Berry, G. T.; Ferreira, C.; Freeze, H. H.; Gahl, W. A.; Nickander, K. K.; Sharer, J. D.; Watson, C. M.; Wolfe, L.; Raymond, K. M. Mol. Genet. Metab. 2018, 124 (1), 82−86.

(2) Reiding, K. R.; Bondt, A.; Hennig, R.; Gardner, R. A.; O'Flaherty, R.; Trbojevic-Akmacic, I.; Shubhakar, A.; Hazes, J. M. W.; Reichl, U.; Fernandes, D. L.; Pucic-Bakovic, M.; Rapp, E.; Spencer, D. I. R.; Dolhain, R. J. E. M.; Rudd, P. M.; Lauc, G.; Wuhrer, M. Mol. Cell. Proteomics 2019, 18 (1), 3−15.

(3) Kotsias, M.; Kozak, R. P.; Gardner, R. A.; Wuhrer, M.; Spencer, D. I. R. PLoS One 2019, 14 (1), No. e0210759.

(4) Vreeker, G. C. M.; Bladergroen, M. R.; Nicolardi, S.; Mesker, W. E.; Tollenaar, R. A. E. M.; van der Burgt, Y. E. M.; Wuhrer, M. Talanta 2019, 205, 120104.

(5) Qu, L.; Jiang, Y.; Huang, X.; Cui, M.; Ning, F.; Liu, T.; Gao, Y.; Wu, D.; Nie, Z.; Luo, L. J. Agric. Food Chem. 2019, 67 (40), 11256−11261.

(6) Wang, H.; Zhao, X.; Huang, Y.; Liao, J.; Liu, Y.; Pan, Y. Analyst 2020, 145 (6), 2168−2175.

(7) Powers, T. W.; Neely, B. A.; Shao, Y.; Tang, H.; Troyer, D. A.; Mehta, A. S.; Haab, B. B.; Drake, R. R. PLoS One 2014, 9 (9), No. e106255.

(8) Powers, T. W.; Holst, S.; Wuhrer, M.; Mehta, A. S.; Drake, R. R. Biomolecules 2015, 5 (4), 2554−2572.

(9) Everest-Dass, A. V.; Briggs, M. T.; Kaur, G.; Oehler, M. K.; Hoffmann, P.; Packer, N. H. Mol. Cell. Proteomics 2016, 15 (9), 3003−3016.

(10) Scott, D. A.; Casadonte, R.; Cardinali, B.; Spruill, L.; Mehta, A. S.; Carli, F.; Simone, N.; Kriegsmann, M.; Del Mastro, L.; Kriegsmann, J.; Drake, R. R. Proteomics: Clin. Appl. 2019, 13, 1800014.

(11) Briggs, M. T.; Condina, M. R.; Ho, Y. Y.; Everest-Dass, A. V.; Mittal, P.; Kaur, G.; Oehler, M. K.; Packer, N. H.; Hoffmann, P. *Proteomics* **2019**, *19*, 1800482.

(12) Drake, R. R.; McDowell, C.; West, C.; David, F.; Powers, T. W.; Nowling, T.; Bruner, E.; Mehta, A. S.; Angel, P. M.; Marlow, L. A.; Tun, H. W.; Copland, J. A. *J. Mass Spectrom.* **2020**, *55*, No. e4490.

(13) Heijs, B.; Holst-Bernal, S.; de Graaff, M. A.; Briaire-De Bruijn, I. H.; Rodriguez-Girondo, M.; van de Sande, M. A. J.; Wuhrer, M.; McDonnell, L. A.; Bovee, J. V. M. G. *Lab. Invest.* **2020**, *100*, 1252.

(14) Jovanovic, M.; Peter-Katalinić, J. *J. Mass Spectrom.* **2016**, *51* (2), 111−122.

(15) Huang, C.; Yan, J.; Zhan, L.; Zhao, M.; Zhou, J.; Gao, H.; Xie, W.; Li, Y.; Chai, W. *Anal. Chim. Acta* **2019**, *1071*, 25−25.

(16) Harvey, D. J. *Mass Spectrom. Rev.* **2020**, *39*, 586−679.

(17) Holst, S.; Heijs, B.; de Haan, N.; van Zeijl, R. J. M.; Briaire-De Bruijn, I. H.; van Pelt, G. W.; Mehta, A. S.; Angel, P. M.; Mesker, W. E.; Tollenaar, R. A.; Drake, R. R.; Bovée, J. V. M. G.; McDonnell, L. A.; Wuhrer, M. *Anal. Chem.* **2016**, *88* (11), 5904−5913.

(18) Pongracz, T.; Wuhrer, M.; de Haan, N. *Molecules* **2019**, *24* (19), 3617.

(19) Zhao, X.; Huang, Y.; Ma, G.; Liu, Y.; Guo, C.; He, Q.; Wang, H.; Liao, J.; Pan, Y. *Anal. Chem.* **2020**, *92* (1), 991−998.

(20) Ruhaak, L. R.; Zauner, G.; Huhn, C.; Bruggink, C.; Deelder, A. M.; Wuhrer, M. *Anal. Bioanal. Chem.* **2010**, *397*, 3457−3481.

(21) Jiao, J.; Yang, L.; Zhang, Y.; Lu, H. *Analyst* **2015**, *140*, 5475−5480.

(22) Soltwisch, J.; Kettling, H.; Vens-Cappell, S.; Wiegelmann, M.; Muthing, J.; Dreisewerd, K. *Science* **2015**, *348*, 211−215.

(23) Bednařík, A.; Bölsker, S.; Soltwisch, J.; Dreisewerd, K. *Angew. Chem., Int. Ed.* **2018**, *57*, 12092.

(24) Niehaus, M.; Robinson, K. N.; Murta, T.; Elia, E. A.; Race, A. M.; Yan, B.; Steven, R. T.; Bunch, J. *J. Am. Soc. Mass Spectrom.* **2020**, DOI: 10.1021/jasms.0c00237, accepted manuscript.

(25) Potthoff, A.; Dreisewerd, K.; Soltwisch, J. *J. Am. Soc. Mass Spectrom.* **2020**, *31*, 1844.

(26) Murray, K. K.; Russell, D. H. *J. Am. Soc. Mass Spectrom.* **1994**, *5*, 1−9.

(27) Niehaus, M.; Soltwisch, J. *Sci. Rep.* **2018**, *8*, 7755.

(28) Boskamp, M. S.; Soltwisch, J. *Anal. Chem.* **2020**, *92* (7), 5222−5230.

(29) Soltwisch, J.; Heijs, B.; Koch, A.; Vens-Cappell, S.; Höhndorf, J.; Dreisewerd, K. *Anal. Chem.* **2020**, *92*, 8697−8703.

(30) Ellis, S. R.; Soltwisch, J.; Paine, M. R. L.; Dreisewerd, K.; Heeren, R. M. A. *Chem. Commun.* **2017**, *53*, 7246−7249.

(31) Domann, P.; Spencer, D. I. R.; Harvey, D. J. *Rapid Commun. Mass Spectrom.* **2012**, *26* (4), 469−479.

(32) Calvano, C. D.; Cataldi, T. R. I.; Kogel, J. F.; Monopoli, A.; Palmisano, F.; Sundermeyer, J. *J. Am. Soc. Mass Spectrom.* **2017**, *28*, 1666−1675.

(33) Dreisewerd, K.; Schürenberg, M.; Karas, M.; Hillenkamp, F. *Int. J. Mass Spectrom. Ion Processes* **1995**, *141* (2), 127−148.

(34) Knochenmuss, R. *Analyst* **2006**, *131*, 966−986.

(35) Dreisewerd, K. *Chem. Rev.* **2003**, *103*, 395−425.

(36) Hamm, G.; Bonnel, D.; Legouffe, R.; Pamelard, F.; Delbos, J.-M.; Bouzom, F.; Stauber, J. *J. Proteomics* **2012**, *75* (16), 4952−4961.

(37) Heijs, B.; Tolner, E. A.; Bovée, J. V. M. G.; van den Maagdenberg, A. M. J. M.; McDonnell, L. A. *J. Proteome Res.* **2015**, *14* (12), 5348−5354.

(38) Taylor, A. J.; Dexter, A.; Bunch, J. *Anal. Chem.* **2018**, *90* (9), 5637−5645.

(39) Shariatgorji, M.; Nilsson, A.; Fridjonsdottir, E.; Vallianatou, T.; Källback, P.; Katan, L.; Sävmarker, J.; Mantas, I.; Zhang, X.; Bezard, E.; Svenningsson, P.; Odell, L. R.; Andrén, P. E. *Nat. Methods* **2019**, *16*, 1021−1028.

(40) Leite, J. F.; Hajivandi, M. R.; Diller, T.; Pope, R. M. *Rapid Commun. Mass Spectrom.* **2004**, *18*, 2953−2959.

(41) Lee, C.; Lu, I.-C.; Hsu, H. C.; Lin, H.-Y.; Liang, S.-P.; Lee, Y.-T.; Ni, C.-K. *J. Am. Soc. Mass Spectrom.* **2016**, *27*, 1491−1498.

(42) Harvey, D. J.; Scarff, C. A.; Crispin, M.; Scanlan, C. N.; Bonomelli, C.; Scrivens, J. H. *J. Am. Soc. Mass Spectrom.* **2012**, *23* (11), 1955−1966.

(43) Heijs, B.; Holst, S.; Briaire-De Bruijn, I. H.; van Pelt, G. W.; de Ru, A. H.; van Veelen, P. A.; Drake, R. R.; Mehta, A. S.; Mesker, W. E.; Tollenaar, R. A.; Bovée, J. V. M. G.; Wuhrer, M.; McDonnell, L. A. *Anal. Chem.* **2016**, *88* (15), 7745−7753.

(44) Harvey, D. J. *J. Am. Soc. Mass Spectrom.* **2005**, *16* (5), 631−646.